

Numerical Modeling of the Rotor Movement in a Permanent-Magnet Stepper Motor

Jan Škofic¹ and Miha Boltežar²

¹Iskra-Mehanizmi, 4245 Kropa, Slovenia, jan.skofic@iskra-mehanizmi.si

²Faculty of Mechanical Engineering, University of Ljubljana, 1000 Ljubljana, Slovenia, miha.boltezar@fs.uni-lj.si (corresponding author)

Cite as: J. Škofic, M. Boltežar: Numerical modelling of the rotor movement in a permanent-magnet stepper motor. IET Electric Power Applications, 2014, 8, (4), pp. 155 – 163, doi: 10.1049/iet-epa.2013.0274

Abstract—This manuscript deals with predicting the dynamic behavior of the rotor in a claw-poled, permanent-magnet (PM), stepper motor. The FEM model of a prototype stepper is used to calculate the magnetic forces on the rotor, where the PM is modeled with an altered geometry approach. This altered geometry helps achieving a realistic magnetic flux density profile and direct PM material property input. The obtained forces are used in the following analysis as the excitation, to simulate the rotor’s rotational and also axial movements with the help of proposed system of equations. To validate the introduced modeling approach, a measurement of the rotational and axial movement was performed on a motor with the same geometry and material properties. The results of the simulated movement are in good agreement with the experimental data for the tested motor.

Keywords—Stepper motors, Permanent magnet motors, Finite-element method, Magnetostatics, Torque, Movement simulation, Position measurement, Velocity measurement.

Highlights:

- Altered geometry PM modeling approach.
- Calculation and reconstruction of torque-displacement curves.
- Upgraded system of equations for simulating the rotational and axial movements of the rotor.
- A robust, computationally efficient, step-by-step simulation method.

I. INTRODUCTION

Small, claw-poled, PM, steppers are commonly used in many home appliances and the automotive industry due to their positioning abilities and their low cost. The performance of the motor is defined by the materials used and its geometrical details, particularly the stator poles. Optimizing the geometry in order to achieve a higher torque can affect the stepping accuracy and the dynamics of the rotor’s movement. Numerous analyses and papers investigating the characteristics of low-cost, PM, steppers have been made in the past using 2D and 3D FEM [1], [2], [3]. The researchers were mainly interested in the static torque characteristics [2], [3], [4], such as pole-shape optimization for maximizing the torque [5] and minimizing the detent [5], [6], investigating the effects of material deterioration [7], [8], the stator-to-stator gap [9] and different magnetization processes [5], [6]. In addition to those useful contributions, some detailed analyses of full-scale motors (without the use of symmetry to reduce the problem size) and their dynamic properties [10], [11] (e.g., eddy currents [12], [13], iron losses [13], stepping [14], [11], pull-in and pull-out [14]) have been made.

This manuscript focuses on the rotor movement, and therefore previous publications and methods serve as the foundation, necessary for a dynamics simulation. The rotational movement of the rotor is traditionally simulated by using the well-established differential equations described in [15] and [16]. This method approximates the torque of the motor with a sine wave [17], [18] and therefore loses some of the valuable

information held by realistic torque-displacement curves. These curves are unique to the individual stator geometry and therefore very important. The problems are avoided if the coupled electro-magnetic-mechanical FEM time-stepping [10] approach (e.g. Ansys Maxwell,) is used. Such approach is highly accurate but computationally demanding and time consuming, due to the large number of FEM calculation iterations. To simulate the effects of the geometry on the stepping abilities of the motor, with a good balance between accuracy and time consumption, an integrated method is proposed in this manuscript. This method combines FEM-calculated magnetic torques and forces with a proposed system of equations, to simulate the rotor's rotational and also axial movements. Firstly, the FEM is used to compute the static torque-displacement and force-displacement curves. The proposed system of equations then uses these curves for quick and independent movement simulations. The axial movement is normally neglected in simulations, due to the small influence on the rotational output. But the axial movement [19] is not so unimportant in small, claw-poled steppers, because of the vibrations and noise that the rotor creates when it axially collides with the bearing flanges. All varying forces excite structures, which then generate changes in the surrounding air pressure, known as acoustic emission (noise). Keeping these excitation forces to a minimum is an efficient way of dealing with noisy structures. These axial vibrations are also problematic when the rotor axis acts as a gear shaft and rotates other gears in small actuators. The system is therefore exposed to an additional wear mechanism and an unpleasant noise that promotes the feeling of low-quality engineering. Therefore, the rotor's axial movement is addressed in this work.

An important aspect of this work is the desire to present the whole workflow as an undemanding, robust and computationally efficient method, for engineers to test their many prototype motors. Therefore this manuscript is organized as follows: In Section II a step-by-step numerical analysis procedure is presented. This incorporates the presentation of the analyzed motor A), the novel modeling of the PM B), torque computation C), introduced rotor's dynamic response equations D) and the design of a simple controller with simulation parameters E). Section III presents experimental setup used to obtain the rotor movement, which is later compared with simulation results in Section IV. The summarized conclusions about the method are given in V.

II. NUMERICAL ANALYSIS PROCEDURE

The creation of a numerical model starts with the CAD geometry of a motor that needs to be virtually tested before the first prototypes are manufactured. The geometry is then imported into Ansys and the material properties are assigned. In order to achieve accurate torque estimations, a non-simplified geometry for all the magnetic parts, except the plain bearings and the shaft, is used. We assume that the stainless-steel shaft and the plain brass bearings do not affect the magnetic flux and do not have a significant influence on the torque characteristics. The PM rotor is modeled as partially stand-alone segments with a radial magnetization that periodically changes direction.

The current in the windings produces a magnetic flux that flows in the stator and polarizes its claw poles. Although the results of the dynamic behavior of the rotor that will be presented in this work corresponds to half-stepping mode, some partial results will show higher order micro-stepping [20] modes for demonstration purposes. For example, full-stepping mode uses only 4 winding-current combinations (4 different torque curves), where 1/16 micro-stepping has 64 combinations (64 different torque curves). In general the method allows simulations of any stepping mode.

By changing the angular position of the rotor, different torque-displacement curves are obtained. These curves represent the potential static torque of the motor. Transient effects are not included in this FEM segment.

The torques and the forces acting on the rotor cause it to move relative to the stator in a manner that is defined by the current available torque and axial force. There is only one useful torque component causing the rotor to rotate (torque about the shaft). Other FEM calculated torques and forces act as unwanted influences that slow down the rotor via the friction of the plain bearings. Using a developed system of differential equations, calculated torques and forces, we can simulate the winding currents, as well as the rotational and axial movement.

In order to simulate a "point-to-point" movement, instead of oscillatory rotation about the first stable position (the zero crossing of an active torque curve), a simple PWM current controller must be simulated. Using the manufacturer's data for a controller phase current output for different movements, a simple

virtual controller can be developed. The controller continuously adjusts the current via the voltage PWM in order to achieve the desired level of current. Changing the current levels changes the torque and the position of the rotor.

A. Prototype-motor specifications

The bipolar, claw-poled, PM, stepper analyzed in this work (Fig. 1a) has 48 poles, corresponding to a 7.5° step angle. In each of the two phases of the stator, a 0.35 mm copper-alloy wire is used for a winding with 160 turns. The stator is formed from structural sheet-metal (normally the stators are made from a magnetic sheet-metal) with an inner diameter of 23 mm and an outer diameter of 42 mm. The permanent magnet made of a bonded Nd-Fe-Co-B powder glued to the rotor has a floor plan of circular ring with the wall thickness of 1.2 mm and height of 11.2 mm. It is magnetized to have 24 poles. The motor is designed to be driven with 0.8 A and ~ 12 V.

B. Permanent-magnet model

Since a low-cost motor is being analyzed here, the PM rotor creates a specific challenge. An Nd-Fe-Co-B magnetic powder is mixed with epoxy resin and injected into a mold to form an economical and effective magnet.

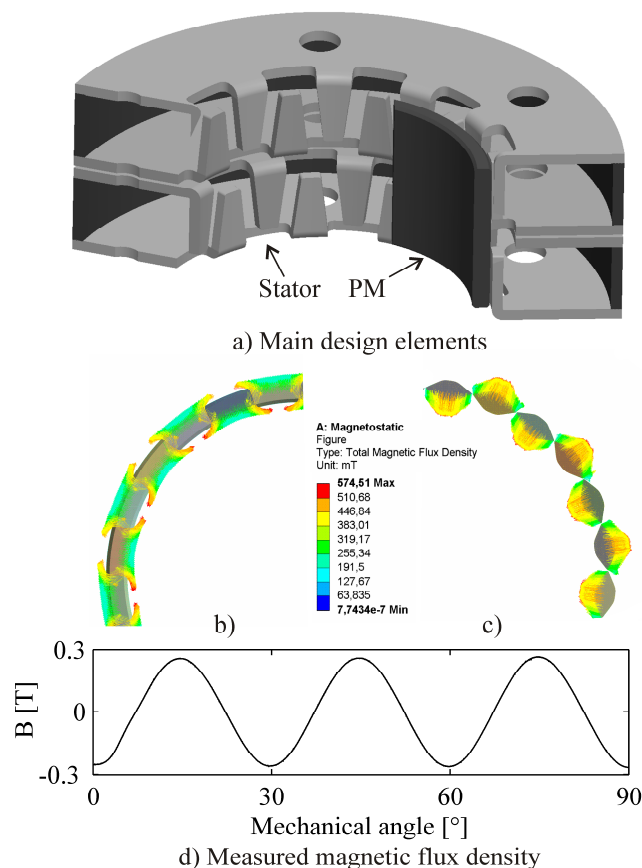


Fig. 1. Main design elements of the motor a). Magnetic flux density profile of a PM: typical segment approach b), proposed geometrical approach c), measured magnetic flux density at approximately 0.15 mm away from the magnet surface d).

However, at this stage the magnet is yet to be magnetized in the magnetizing machine to create the radially magnetized segments which later interact with energized stator. Because there is a considerable amount of resin, air pockets and optionally fibers in the magnet, the energy product, residual induction and coercive force all change respectively to volumetric loading of the magnetic powder (specified by the manufacturer). The real magnetized magnet also has a sinusoidal magnetic flux distribution along its tangential direction (Fig. 1d), which is in slight conflict with the result of the simulation if a simple radial segments of the PM ring are used (Fig. 1b). Due to these problems with the need of scaling the magnetic material properties and obtaining the realistic sinusoidal shaped magnetic density profile (Fig. 1d) a new method for changing the geometry of the PM was developed.

This method proposes that the segment's geometry and volume are changed to suit the volume portion of the magnetic material but keep both original inner and outer PM diameters in its centers (Fig. 1c). The model therefore also keeps the original wall thickness and very important rotor-stator air gap. The shape of the segments is not explicitly defined due to the possible variation of the volumetric loading of magnetic powder and angular width of the segment. For the first approximation the sinusoidal shape of the segments (Fig. 1c) can be used. Afterwards, typically less than 4 iterations are needed to obtain the satisfactory shape that corresponds to the combination of desired volume and the approximate magnetic flux density profile. The magnetic flux density of the newly shaped segments (Fig. 1c) resembles the sinusoidal distribution (Fig. 1d) more closely than the typical approach (Fig. 1b) and also does not need the scaling of material properties. An alternative, but relatively complex approach for improved PM modeling is presented in [7] where the author analyses the magnetization process.

C. Torque computation

The current in the winding generates a magnetic field around the leads/coils. The direction of this rotational field depends on the direction of the current flow. The created magnetic flux runs on the stator metal and polarizes the claw poles. Each pole now attracts a rotor segment of opposite polarization, thereby generating useful torque. Since there is usually a lot of interest in design influences [2], [5], a 3D FEM is used to compute these torques and forces in multiple rotor positions. The torque-displacement curves hold much information about the performance of the motor. The peak torque and zero-crossing locations determine the strength and stepping accuracy of the motor. Because the main interest is dynamics, the shape of the curve is also crucial. Computing the torque with the FEM is an accurate (often used for different model verifications [21]) and flexible [8] way to calculate the torque behavior. Influences such as temperature, teeth bending stresses [8] and manufacturing errors can be easily simulated. Based on the phase-current levels in the desired stepping mode (Fig. 2), a torque-displacement curve is calculated (Fig. 3a). Because of the motor's geometry, the torque curve repeats 12 times in one rotor rotation. This means that it is only necessary to calculate the torque values for 30 degrees of rotation. Using a periodic expansion the torque curve (Fig. 3a) can be extended to suit specific needs (Fig. 3b). To define the static properties of the full-stepping mode a total of four torque-displacement curves need to be calculated. These are defined by [566; -566], [566; 566], [-566; 566], [-566; -566] mA (800 mA of a total driving-current), respectively, to signals in Fig. 2a. For half (Fig. 2b), quarter, etc. stepping, the required number of curves quickly increases. For example, the curves represented in the 1/8-stepping mode are shown in Fig. 3c.

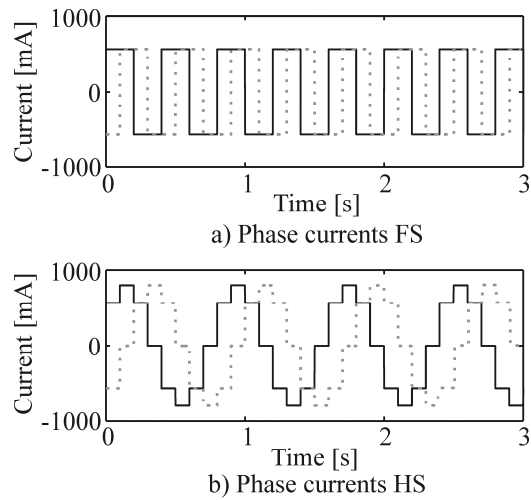


Fig. 2. Full-stepping signal a) and half-stepping signal b).

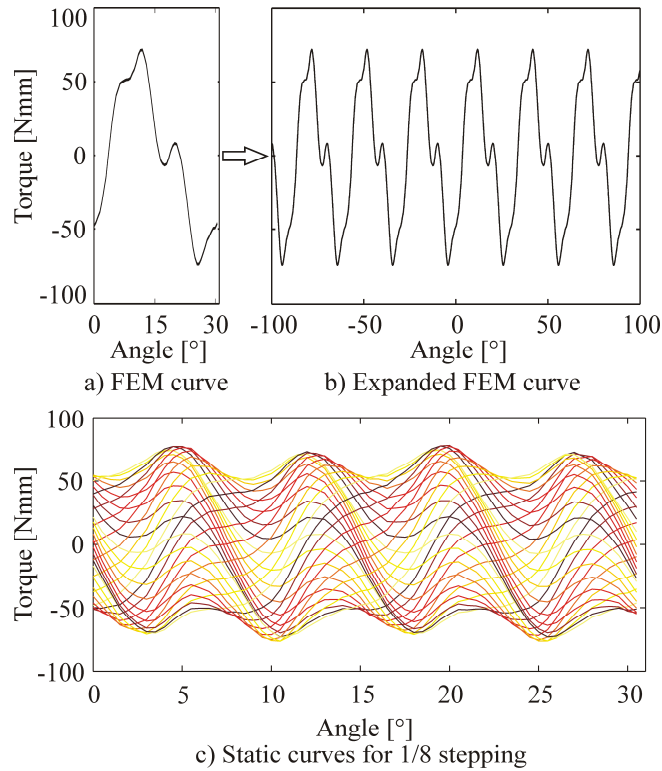


Fig. 3. Representation of torque-displacement curves. Curve obtained with magnetostatic FEM at [800; 0] mA a), periodically expanded curve b), curves representing 1/8 micro-stepping mode c).

Computing these curves can be time consuming due to the number of elements needed to achieve accurate results. Some reduction in the number of elements can be achieved by using a virtual work method and a vector potential [22]. The number of needed elements can be determined by recalculating the same point several times with an increasing number of elements to see where the solution converges. By using this method, it is possible to decide how many elements are sufficient for an accurate, individual analysis, and then the best balance between accuracy and computing effort can be found.

Because the FEM curves are static, the removed material from the rotor does not present any drawbacks. Realistic mass and inertia will be used as constants in an independent dynamics simulation.

Obtaining a large number of torque curves for high division stepping modes (e.g. 32 curves for 1/8 or 64 for 1/16-stepping mode) with a sufficient quantity of finite elements is time consuming and therefore unpractical. To overcome this problem, most of the curves can be reconstructed from the four primary curves c16, c32, c48, c64 shown in Table I. Table I presents the phase currents defining the torque-displacement curves (c1-c64) for the 1/16 micro-stepping mode (skipping every second combination will give 32 combinations corresponding to 1/8 micro-stepping mode, etc.). A total of 64 curves can be obtained by calculating only c16, c32, c48 and c64 (Table I). These are the primary curves, where the maximum phase current energizes only one phase of the motor. The current in the other phase is set to zero.

TABLE I: All static torque curves for 1/16-stepping defined by phase currents in amperes

curve	C1	C2	...	C15	C16	C17	...	C31	C32	C33	...	C47	C48	C49	...	C63	C64
I_1 [A]	0.078	0.156			0.8				0				-0.8				0
I_2 [A]	-0.796	-0.785			0				0.8				0				-0.8

The reconstruction of the other curves can be made using the introduced equations (1)–(4), where c1–c64 are the torque vectors, cX is the reconstructed torque vector, n is the n -th vector element, I_1 is the current in the first phase and I_2 is the current in the second phase.

c1 – c15:

$$cX(n) = c64(n) \cdot |I_2(cX)| + c16(n) \cdot |I_1(cX)| \quad (1)$$

c17 – c31:

$$cX(n) = c16(n) \cdot |I_1(cX)| + c32(n) \cdot |I_2(cX)| \quad (2)$$

c33 – c47:

$$cX(n) = c32(n) \cdot |I_2(cX)| + c48(n) \cdot |I_1(cX)| \quad (3)$$

c49 – c63:

$$cX(n) = c48(n) \cdot |I_1(cX)| + c64(n) \cdot |I_2(cX)| \quad (4)$$

For example (Fig. 4), a c2 torque curve with $I_1=156$ mA and $I_2=-785$ mA can be reconstructed from c16 and c64 with equation (1) in $n=1:62$ points (0.5 degrees increment).

The primary curves were computed with FEM and the use of B-H curve for the metal, so they include the detent torque and saturation effects. Because the reconstruction expressions (1)–(4) produce torque curves that are only a linear combination of the primary ones, we can expect some minor discrepancies compared to a FEM calculated curve (Fig. 4). This reduction of quality is a simplification made to speed-up the simulations.

An additional speed-up of the computation of the torque-displacement curves can be achieved by computing only one primary curve and offset the other three for the appropriate displacement angle. It is advised to compute all four primary curves for the first prototype motor to find the right angle offset.

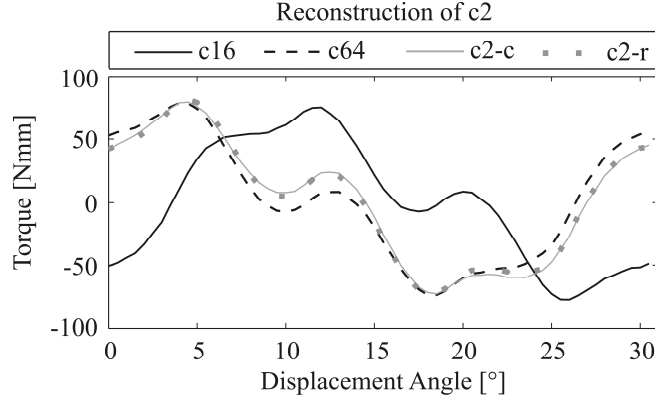


Fig. 4. Reconstructed torque curve c2-r and FEM computed c2-c.

An investigation of the zero-crossing of the torque-displacement curves lets us examine the stepping accuracy of the motor. This is very useful pre-manufacturing data, because of the well-known problems with the stepping accuracy of claw-poled, PM, steppers in micro-stepping modes. The gradient of the curve at zero-crossing defines the motor's ability to secure the step position. A steep curve is important in applications where a high operating friction is expected, because the positioning will be more accurate. The gradient also affects the oscillating frequency of the rotor. The shape of the curve affects the rotor's rotational movement. A high torque ripple (Fig. 3c) causes the rotor to run more roughly.

The same procedure for the computation and reconstruction can be used to determine the axial forces on the rotor.

D. Computation of the rotor's dynamic response

A well-established method for simulating the rotor movement for hybrid and claw-poled steppers is to solve a system of differential equations described in [15], [16]. This method is a fast and robust means of simulating the rotor movement and the stepper's dynamic characteristics, such as pull-in and pull-out [15]. The drawback of this method is the sinusoidal simplification. The torque generated by energizing the stator is assumed to be a sine wave, which is rarely the case in claw-poled steppers (see section II.C). In addition, the motor's torque and detent constants have to be obtained. These are highly important as they define the shape of the torque-displacement curve. So they have to be either measured or computed by other means. In present times of modern computers these drawbacks present a good argument for using FEM.

Simulating the movement by recalculating the forces with the FEM after each time step dt is a time-consuming method, because of the large number of steps necessary to appropriately simulate the "point-to-point" movements. The results are accurate [10] because it is possible to include electromagnetic coupling, eddy-current and iron losses [12], [13] that influence the magnetic field generation, especially at high stepping rates (e.g. Ansys Maxwell). Whereas this approach is well suited for individual analyzes (e.g., in detailed scientific researches and in "cutting" edge applications), its drawbacks are evident when a wider range of motors is being analyzed. Namely, large computation demands and times limit the applicability of the approach in parametric studies and optimization procedures, where a greater number of analyzes is required.

The approach introduced in this manuscript joins both methods to develop a relatively fast and accurate method for the numerical simulations of stepper motors. The developed system of equations (derived from [15], [16]) uses torque-displacement and force-displacement curves, to simulate both the rotational and axial movement of the rotor. Once the FEM curves are obtained and stored, any movement can be quickly simulated with the introduced system of equations (5)–(9), independently of FEM model:

$$\frac{di_1}{dt} = \left[u_1 - R \cdot i_1 - M \cdot \frac{di_2}{dt} + \omega \cdot TC_{1,0}(\Theta) \right] / L_1 \quad (5)$$

$$\frac{di_2}{dt} = \left[u_2 - R \cdot i_2 - M \cdot \frac{di_1}{dt} + \omega \cdot TC_{0,1}(\Theta) \right] / L_2 \quad (6)$$

$$\frac{d\omega}{dt} = \frac{1}{J} \cdot [T(i_1, i_2, \Theta) - B_r \cdot \omega - \text{sgn}(\omega) \cdot (T_e + T_a + T_z)] \quad (7)$$

$$\frac{dz}{dt} = \frac{1}{m_r} \cdot [F_z(i_1, i_2, \Theta) - B_a \cdot \dot{z} - \text{sgn}(\dot{z}) \cdot \left(g \cdot m_r \cdot \mu_a + \frac{T_e}{r_s} \right) - c_{sw} \cdot z] \quad (8)$$

$$\frac{d\Theta}{dt} = \omega, \quad (9)$$

where i_1, i_2 are the currents in both phases, u_1, u_2 are the voltages, R is the winding resistance, M is the mutual inductance of the windings, L is the winding inductance (In particular case both L and M are obtained by FEM. Inductances are many times considered independent of rotation θ [15], [16], however a FEM computation enables a θ dependent L and M to be obtained and used for even more accurate analyses), ω is the rotor angular velocity, $TC_{l,o}(\theta)$ is the torque curve calculated with the FEM, when only one winding is fully energized (note that it must be calculated with 1A winding current or normalized to 1A to satisfy unit requirements), θ is the rotor position, J is the rotor inertia, $T(i_1, i_2, \theta)$ is the torque defined by (1)–(4) for a current rotor position, T_e is the friction torque generated by the rotor's mass eccentricity, T_a is the friction torque added to the motor (gearbox, encoder, etc.), T_z is the friction torque caused by the rotor's axial movement (10), \dot{z} is the rotor's axial velocity, m_r is the mass of the rotor, $F_z(i_1, i_2, \theta)$ is the axial force for the current rotor position (defined in a similar way to the torque), g is the acceleration due to gravity (in current application the motor's axis lays in horizontal plane (Fig. 5)), μ_r is the coefficient of friction between the plain brass bearing and the stainless-steel shaft, c_{sw} is the spring-washer spring constant, B_r is the rotational movement damping constant (for more information on damping properties please see [12], [16], [23-27]), B_a is the axial movement damping constant and z is the axial displacement of the rotor.

Spring washers help maintain the axial position of the rotor, and so contribute to the good vibro-acoustic aspects of the product. The axial movement of the rotor, governed by newly formulated equation (8), causes the compression of either the upper or lower spring washer. Compression creates a friction torque T_z that affects the rotation. In (10) r_{bf} represents the mean radius of the bearing flange and μ_a is the axial friction coefficient.

$$T_z = c_{sw} \cdot z \cdot r_{bf} \cdot \mu_a \quad (10)$$

$$T_e = m_r \cdot r_e \cdot \omega^2 \cdot \mu_r \cdot r_s \quad (11)$$

The friction torque caused by the mass eccentricity of the rotor T_e is described by (11), where r_e is the eccentricity and r_s is the shaft radius. The mass eccentricity should not be confused with geometrical run-out of the rotor. The run-out would affect the magnetic field and change the FEM calculated curves.

E. Virtual controller

Without the ability to control the winding currents a rotor only moves to the nearest stable point and holds its position with a holding torque. Different combinations of winding currents change the shape of the torque-displacement curves and therefore the stable positions, so the motor can step in the desired direction. The higher the micro-stepping mode, the higher the number of different torque combinations to consider. If the controller sets a constant time interval for all the current combinations, a motor will be stepping at a constant rate. Shortening the time intervals speeds up the rotation and the stepping becomes smoother and more coherent. If the intervals become too short, the rotor can no longer keep up with the fast-changing magnetic field defined by the stator and the motor loses synchronization. To avoid any loss of synchronization (step loss), a careful analysis must be made. In contrast, elongating the intervals causes deceleration. This work deals with two different simulations.

For the stepping test, the controller has to change the current in the windings each tenth of a second in order to engage the next torque curve. This test reveals the stepping accuracy and the “ringing” (overshoots and undershoots) characteristics of the motor.

The test of two rotations with a linear acceleration profile is meant to examine the theoretical dynamic behavior of high speed rotational movement. The 192 steps in the 1/2-stepping mode define a theoretical 720° rotation. Such point-to-point movements with a linear acceleration profile are common tasks for steppers in many positioning systems. The simulation parameters are presented in Table II.

TABLE II: Simulation parameters

V_{\max}	973 PPS (full-step)
V_{\min}/V_{\max}	15/32
Acceleration	19092 full-step/s ²
Stepping mode (SM)	1/2
I_{run}	800 mA

Micro-stepping gives steppers the ability to run more smoothly with less torque ripple and therefore less vibration. The speed of the stepper is in most cases stated in PPS (positions per second), which relates to RPM (rotations per minute), as stated in (12), where $2p$ is the number of motor poles.

$$v_{RPM} = \frac{v_{PPS} \cdot 60^\circ}{2p} \quad (12)$$

III. EXPERIMENT

To evaluate the simulation results an experiment with stepping and point-to-point movement was made. The motor was driven with an AMIS-30623, bipolar, stepper-motor chip based on LIN communication (automotive CAN standard sub frame).

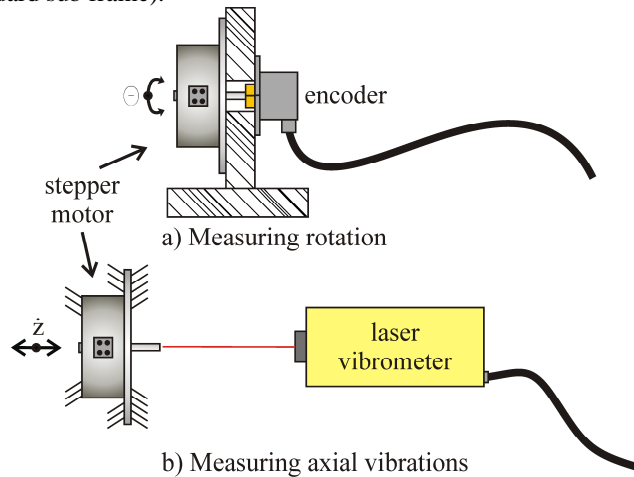


Fig. 5. Experimental setup. Measuring rotational movement with encoder a), and axial vibrations with vibrometer b).

The shaft of the motor was coupled with a Scancon miniature encoder using 10^{-7} kgm² of inertia and 0.5 Nmm of friction torque (Fig. 5a). The encoder has a resolution of 7500 lines per rotation, which is then

multiplied by four in the measuring software. Axial movement was measured using a Polytec portable digital vibrometer PDV-100, with the sensitivity of 5(mm/s)/V. The beam of a helium neon laser was pointed in the center of the motor shaft to precisely measure the axial velocity without adding any mass [28] to a very light rotor (Fig. 5b). A non-contact measurement of axial movement was performed without the presence of encoder, so the rotor was able to move freely. The data acquisition was performed with a 20 kHz sampling frequency.

IV. COMPARISON AND DISCUSSION

The validation of the proposed method was started with a simulation of the stepping. Each tenth of a second the controller sets a new phase-current combination, which defines a new torque curve with a different zero crossing. The rotor reacts to the change in the torque and moves to a new, stable position. Fig. 6 shows 12 consecutive steps in $\frac{1}{2}$ -stepping mode. Theoretically, the step angles should be 3.75° and all equal. In this case the non-optimal stator geometry causes unwanted anomalies in the torque curves, which affect the motor's stepping abilities. A combination of short and long steps is a common problem when micro-stepping a claw-poled, PM, steppers. For that particular reason Fig. 6 shows $\frac{1}{2}$ -stepping instead of full-stepping mode. Comparison of the simulation (Fig. 6a) and measurement (Fig. 6b) of a stepping accuracy test in $\frac{1}{2}$ -stepping mode reveals a relatively good quality of the simulation. 12 consecutive steps are enough to see the motors poor stepping abilities.

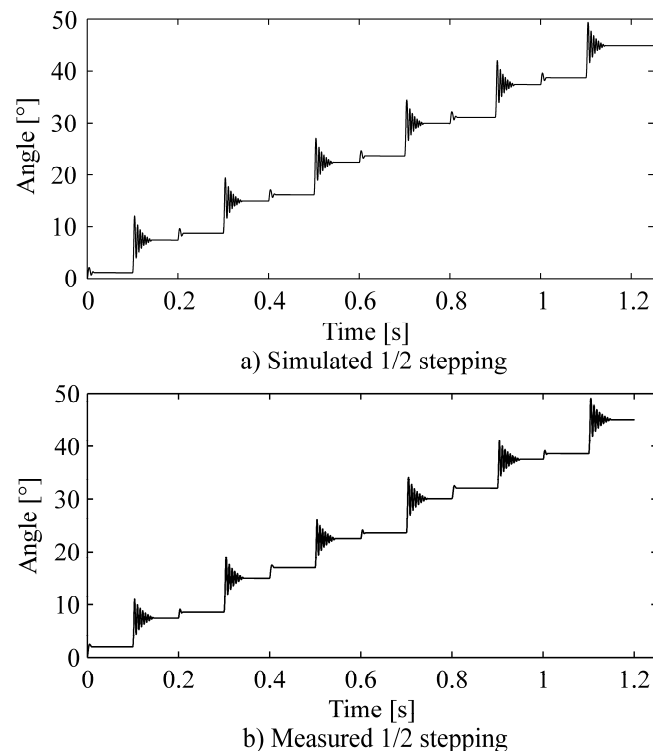


Fig. 6. Simulation a) and measurement b) comparison of the $\frac{1}{2}$ -stepping.

The point-to-point movement was specially chosen to incorporate acceleration, continuous run, deceleration, and damped oscillation during the final step for comparison purposes. The plot of angular displacement (Fig. 7a-c) mainly shows the final (delivery) position, the information about the time necessary to reach the position and the overshoot at the last step. Fig. 7d shows more detailed information about the acceleration, constant speed and deceleration. Inspecting both plots (Fig. 7a and Fig. 7d) gives the engineer important information about the rotational behavior of the motor.

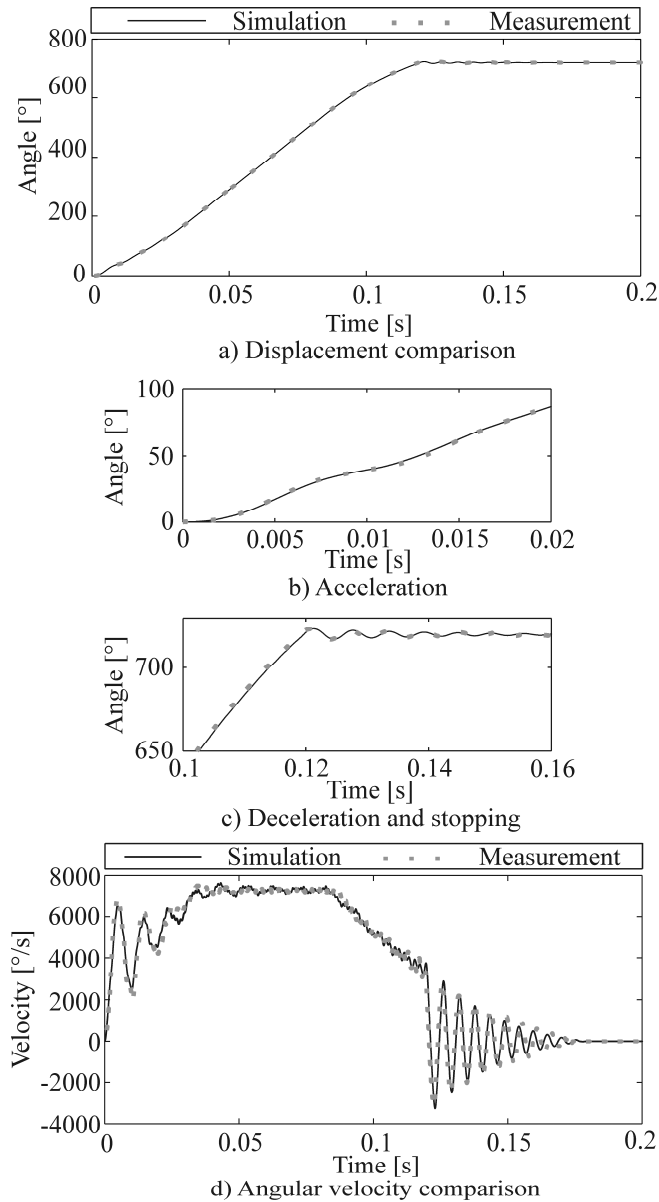


Fig. 7. Simulation and measurement comparison for the point-to-point movement a), with detailed views for the acceleration b) and deceleration c). Angular velocity comparison is shown in d).

Fig. 7a shows the comparison of the experimentally obtained and simulated rotor displacement. Due to the marginal discrepancies, the acceleration and deceleration are checked separately. Fig. 7b is focused on the acceleration, where the rotor quickly gains speed and synchronizes with the stator-generated flux. Fig. 7c shows a combination of the rotor's deceleration and the damped oscillation.

The quality of the simulation can be more accurately viewed with a plot of the angular velocity (Fig. 7d). Small deviations of the simulation compared to the measurements are more obvious when comparing the derivatives. The simulation fails to completely imitate the measurement at the peaks and the local minima of the acceleration (0–0.03 s). Also, the frequency of the synchronization in the simulation appears to be higher than in the experimental data. This can be the cause of the minimal errors in the total inertia or the rotating parts, the calculated torque, the frictional and the damping parameters. The differences are gradually minimized when the rotor reaches its designated speed (0.03–0.08 s). Deceleration (0.08–0.12 s) and damped oscillations (0.12–0.17 s) at the final step can be very problematic to simulate in small steppers. As is clear from the stepping analysis, drastic differences between the individual steps are

possible. Combining that with the non-uniform friction, which depends on the angular location due to assembly errors when coupling the shaft with the encoder, can result in very different behaviors.

During the rotation the rotor also moves axially (Fig. 8). This simulation and also experiment were carried out using spring washers on both sides of the rotor, which hold the rotor centered between the bearings and improve the vibro-acoustics of the motor, especially at low stepping rates. Without the use of the washers some impacts occur between the rotor and the bearings. To simulate the axial movement in the motor without spring washers, (8) should be altered appropriately. The simulation produces results that are in a good agreement with experimentally obtained data (Fig. 8). Again, the most problematic section is the synchronization at acceleration (~ 0.015 s), with similar reasons as stated for the rotational velocity. The frequency domain analysis (Fig. 8) confirms a good agreement.

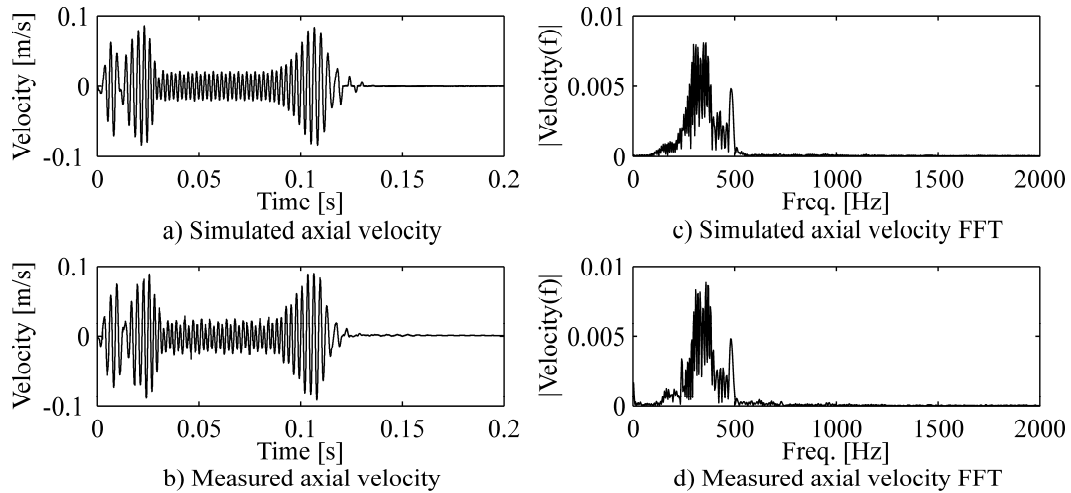


Fig. 8. Axial velocity comparison.

V. CONCLUSIONS

This manuscript presents an integrated step-by-step approach with a different PM modeling preposition and introduced coupled rotational-axial movement equations to simulate the rotor movement in PM steppers. The method is designed as an engineering tool for analyzing the geometrical influences of prototype motors, creating large parametric studies and optimizations, with a favorable combination of computing effort and simulation quality. Through the use of FEM, PM modeling approach and broad energy-dissipation mechanisms, we minimize the need for an iterative search for the right simulation parameters. The method also incorporates the ability to simulate the axial movement of the rotor, and so enables the additional experimentation of the vibro-acoustic aspects of the motor. A step-by-step open approach is also beneficial for using only part of the method. When the focus is on the static characteristics of the motor, it is only necessary to calculate the primary torque curves and reconstruct the others. In this way the torque characteristics and the potential stepping accuracy are known. On the other hand, if the torques and forces are already established, only the proposed dynamic equations can be used to simulate the movement. With regards to experimental data, the introduced approach displayed the accuracy, sufficient for the majority of engineering applications.

ACKNOWLEDGMENT

With special thanks to prof. Janez Diaci. Operation is partly financed by the European Union, European Social Fund.

REFERENCES

- [1] Oswald, A., Herzog, H. G.: 'Investigation of the usability of 2d-and 3d-fem for a hybrid stepper motor'. Proc. IEEE Int. Elect. Mach. Drives Conf., IEMDC '09, Miami, FL, May 2009, pp. 535-542
- [2] Ahn, J. H., Park, S. C., Rhyu, S. H., Jung, I. S.: 'Claw-pole shape design of permanent magnet stepping motor'. Proc. 8th Int. Conf. Elect. Mach. Syst., ICEMS 2005, Nanjing, China, Sept. 2005, pp. 276-279
- [3] Jung, D. S., Lim, S. B., Kim, K. C., *et al.*: 'Optimization for improving static torque characteristic in permanent magnet stepping motor with claw poles'. IEEE Trans. Magn., Apr. 2007, 43, (4), pp. 1577-1580
- [4] Liu, C. P., Li, Y. C., Liu, K. H., Wu, K. T., Yao, Y. D.: 'Analysis of the performance of permanent magnetic stepping motor with trapezoid stator tooth'. J. Appl. Physics, Apr. 2006, 99, (8), pp. 08R316-08R316-3
- [5] Ishikawa, T., Takakusagi, R., Matsunami, M.: 'Static torque characteristics of permanent magnet type stepping motor with claw poles'. IEEE Trans. Magn., 36, (4), July 2000, pp. 1854-1857
- [6] Lim, S. B., Jung, D. S., Kim, K. C., Koo, D. H., Lee, J.: 'Characteristic analysis of permanent-magnet-type stepping motor with claw poles by using 3 dimensional finite element method'. IEEE Trans. Magn., 43, (6), June 2007, pp. 2519-2521
- [7] Hattori, T., Suzuki, Y., Yamada, T.: 'Analysis of permanent magnet type stepping motor with claw poles using electromagnetic field analysis'. Proc. Int. Conf. Elect. Mach. Syst., ICEMS 2008, Wuhan, China, Oct. 2008, pp. 3539-3543
- [8] Okada, Y., Kawase, Y., Hisamatsu, Y.: 'Analysis of claw-poled permanent magnet-stepping motor considering deterioration of material characteristics by remains stress'. IEEE Trans. Magn., May 2003, 39, (3), pp. 1721-1724
- [9] Liu, C. P., Jeng, G. R., Chen, W.C., Tsai, M. C., Wu, K. T., Yao, Y. D.: 'Performance of claw-poled pm-stepping motor'. J. Magn. Magn. Mater., 2007, 310, (2), pp. e910-e912
- [10] Jabbar, M., Liu, Z. Dong, J.: 'Time-stepping finite-element analysis for the dynamic performance of a permanent magnet synchronous motor'. IEEE Trans. Magn., Sept. 2003, 39, (5), pp. 2621-2623
- [11] Rhyu, S., Kwon, B., Jung, I. S.: 'Dynamic characteristic analysis of small sized pm type stepping motor with h shape stator yoke'. Proc. Conf. Elect. Field Computation, Miami, FL, 2006, pp. 248-248
- [12] Suzuki, S., Kawase, Y., Yamaguchi, T., Yoshimura, T., Hirata, K., Ota, T.: 'Dynamic characteristics analysis of claw-poled stepping motor employing 3-d finite element method'. Proc. Int. Conf. Elect. Mach. Syst. ICEMS 2009., Tokyo, Japan, Nov. 2009, pp. 1-4
- [13] Zhu, Z., Jewell, G., Howe, D.: 'Finite element analysis in the design of permanent magnet machines'. Proc. IEE Seminar on Current Trends in the Use of Finite Elements in Elect. Mech. Des. Anal., London, England, 2000, pp. 1/1-1/7
- [14] Rhyu, S., Jung, I., Hur, J., Kwon, B.: 'Development of a 4.0 mm-outer-diameter pm type stepping motor with a newly structured claw-poles'. Proc. Int. Conf. Elect. Mach. Syst., ICEMS 2007, Seoul, Korea, 2007, pp. 860-863
- [15] Balakrishnan, K., Umamaheswari, B., Latha, K.: 'Estimation of rotor position and speed for hybrid stepper motor under various phase excitation schemes and compensated resonance'. Proc. Int. Conf. Power Eng. Energy and Elect. Drives, Malaga, Spain, May 2011, pp. 1-6
- [16] Hughes, A., Lawrenson, P.: 'Electromagnetic damping in stepping motors'. Proc. Inst. Elect. Eng., Aug. 1975, 122, (8), pp. 819-824
- [17] Kikuchi, T., Kenjo, T., Fukuda, S.: 'Developing an educational simulation program for the pm stepping motor'. IEEE Trans. Edu., Feb. 2002, 45, (1), pp. 70-78
- [18] Sekhara Rao, E. V. C., Prasad, P. V. N.: 'Effect of mid frequency resonance on dynamic response of permanent magnet on hybrid stepper motor'. Proc. Int. Conf. Inform. and Commun. Technol. Elect. Sci., ICTES 2007, Chennai, India, 2007, pp. 431-432
- [19] Nguyen, Q. D., Ueno, S.: 'Modeling and control of salient-pole permanent magnet axial-gap self-bearing motor'. IEEE/ASME Trans. Mechatronics, June 2011, 16, (3), pp. 518-526
- [20] Yeadon, W. H., Yeadon, A. W.: 'Handbook of small electric motors'. (McGraw-Hill, 2001), pp. 10.93-10.96.

- [21] Rossini, L., Chételat, O., Onillon, E., Perriard, Y.: 'Force and torque analytical models of a reaction sphere actuator based on spherical harmonic rotation and decomposition'. *IEEE/ASME Trans. Mechatronics*, June 2013, 18, (3), pp. 1006 - 1018
- [22] De Medeiros, L., Reyne, G., Meunier, G.: 'Comparison of global force calculations on permanent magnets'. *IEEE Trans. Magn.*, Sept. 1998, 34, (5), pp. 3560-3563
- [23] Hughes, A.: 'High-speed operation of stepping motors'. *Electronics and Power*, Oct. 1978, 24, (10), pp. 747-750
- [24] Jassal, A., Polinder, H., Ferreira, J. A.: 'Literature survey of eddy-current loss analysis in rotating electrical machines'. *IET Electr. Power Appl.*, 2012, 6, (9), pp. 743-752
- [25] Song, B.-K., Sun, T., Hong, J.-P., Lee, J.-J.: 'Hysteresis torque estimation by using iron-loss analysis in permanent magnet synchronous motor'. *IET Electr. Power Appl.*, 2011, 5, (7), pp. 558-562
- [26] Ionel, D. M., Popescu, M., Dellinger, S. J., Miller, T. J. E., Heideman, R. J., McGilp, M. I.: 'On the variation with flux and frequency of the core loss coefficients in electrical machines'. *IEEE Trans. Ind. Appl.*, May 2006, 42, (3), pp. 658-667
- [27] Fiorillo, F.: 'Measurement and characterization of magnetic materials'. (Elsevier Academic Press, 2004), p. 31
- [28] Moreno, R., Chicharro, J.M., Pintado, P.: 'Comparison of minimum detectable crack size in a geared system from three different vibration transducer types'. *Experimental Techniques*, Early View (Online Version of Record published before inclusion in an issue), 2011, doi: 10.1111/j.1747-1567.2011.00774.x